

CRYOPRESERVATION OF TISSUE ENGINEERED SKELETAL MUSCLE

BY

LAUREN GRANT

THESIS

Submitted in partial fulfillment of the requirements
for the degree of Master of Science in Bioengineering
in the Graduate College of the
University of Illinois at Urbana-Champaign, 2018

Urbana, Illinois

Adviser:

Professor Rashid Bashir

ABSTRACT

Tissue engineered skeletal muscle plays an important role not only in the field of regenerative medicine, but also in emerging areas such as soft robotics, organ-on-a-chip models of disease, and drug testing. However, further expansion of the applications of tissue engineered skeletal muscle models will require a suitable method for their long-term storage and shipment. Cryopreservation has long been the standard for long-term cell storage, but when it comes to the freezing of 3D tissues, many complications arise due to heat and mass transfer limitations. Here, we use a tissue engineered skeletal muscle bioactuator as a model to characterize the effects of freezing on skeletal muscle viability, gene expression, myotube structure, and force generation. We optimize the freezing medium composition and compare the effects of freezing on both undifferentiated and differentiated engineered skeletal muscle tissue constructs. We report an optimized protocol of freezing skeletal muscle constructs while undifferentiated, which not only maintains cell viability, but leads to a 3-fold increase in force production as compared to unfrozen muscle. The reported timeline for skeletal muscle tissue fabrication, freezing, and revival not only promotes a more streamlined fabrication process, but will further enable collaborative research efforts through the shipment of pre-formed skeletal muscle constructs.

ACKNOWLEDGEMENTS

I would like to first thank my adviser, Professor Rashid Bashir, for his guidance and support throughout the course of this research. I would also like to thank Dr. Ritu Raman, who provided wonderful mentorship and developed much of the groundwork for this research project. I would also like to thank Dr. Caroline Cvetkovic for her mentorship and constant encouragement. I would also like to thank my lab members, Gelson Pagan-Diaz, Eunkyung Ko, and Yongdeok Kim for insightful discussion and much appreciated friendship.

This work was funded by National Science Foundation (NSF) Science and Technology Center Emergent Behavior of Integrated Cellular Systems (EBICS) Grant CBET0939511. I am also grateful to have received funding from NSF Research Traineeship in Understanding the Brain (NRT-UtB): Training the Next Generation of Researchers in Engineering and Deciphering of Miniature Brain Machinery, Grant 1735252, as well as the University of Illinois SURGE (Support for Under-Represented Groups in Engineering) fellowship.

Finally, I would especially like to thank my friends and family, who continuously supported me throughout this process. I could not have done this without them.

TABLE OF CONTENTS

CHAPTER 1: INTRODUCTION.....	1
CHAPTER 2: METHODOLOGY	3
CHAPTER 3: RESULTS	9
CHAPTER 4: DISCUSSION.....	23
CHAPTER 5: CONCLUSIONS AND FUTURE DIRECTIONS	27
REFERENCES	28
APPENDIX A: RT-QPCR PRIMER SEQUENCES.....	30
APPENDIX B: BIOBOT VIDEOS	31

CHAPTER 1: INTRODUCTION

Engineered skeletal muscle tissue has long been of interest to the tissue engineering community, because of its potential to counteract loss of function resulting from volumetric muscle loss injuries or degenerative illness [1], [2]. More recently, efforts to tissue engineer skeletal muscle have targeted applications beyond regenerative medicine, such as organ-on-a-chip models of disease [3]–[5], formation of *in vitro* neuromuscular junctions [6], [7], and cell-based bioactuators for soft robotics [8]–[11]. As these studies generate more functional tissues, with different end use applications, there is a growing need for a robust method of storing engineered skeletal muscle long-term.

Cryopreservation has long been the standard for storing living cells that must be revived post-preservation [12]. While cryopreservation of cell suspensions is a well understood and characterized process, freezing and revival of engineered tissue has not been investigated or optimized with similar rigor, as the protocol must be customized to tissue type [13]. Most cell freezing processes rely on the use of dimethyl sulfoxide (DMSO), a cryoprotectant that inhibits the formation of ice crystals that could lyse cells, in the freezing medium [14]. However, it is unclear whether this medium composition is sufficient for preserving the morphology and function of myoblasts embedded within 3D engineered skeletal muscle tissue. Since this has not been reported in the literature, to our knowledge, there is a need for the growing body of skeletal muscle tissue engineers to understand, optimize, and use a standardized protocol for long-term storage and revival of the tissue.

Engineering mature contractile skeletal muscle can take several days to weeks, depending on the protocol used [15]–[19]. In addition to optimization of freezing medium composition, a

comprehensive study of skeletal muscle cryopreservation also requires investigating a proper timeline for freezing and reviving engineered tissue. This protocol must take into account the maturity of the tissue and the use of undifferentiated myoblasts or differentiated myotubes, and yield an understanding of the advantages and disadvantages of freezing tissue in either state. Moreover, since all end use applications of engineered skeletal muscle will require the tissue to be contractile in response to external stimulation, the effect of cryopreservation on muscle force production must also be well characterized.

This study aims to develop a protocol for freezing and revival of engineered skeletal muscle tissue that keeps the tissue viable, metabolically active, and contractile. By providing a deeper understanding of the optimized timeline for muscle cryopreservation, this protocol promises to generate guidelines for researchers to accomplish long-term storage and revival of skeletal muscle tissue.

CHAPTER 2: METHODOLOGY

2.1 Stereolithographic 3D printing of ring molds and bio-bot skeletons

Molds for the formation of muscle ‘ring’ structures were 3D printed using a modified form of the commercially available stereolithography apparatus (SLA 250/50, 3D Systems), as previously reported [15], [16]. These molds were fabricated using 20% w/v PEGDMA of molecular weight 1000 g mol^{-1} (Polysciences) with 0.5% w/v Irgacure 2959 (Ciba). We used a biological micro robot (biobot) to characterize the forces produced by the muscles [15], [16]. The skeleton of the biobots, onto which the muscle rings are transferred, were fabricated using 20% w/v PEGDA of molecular weight 700 g mol^{-1} (Sigma-Aldrich) with 0.5% w/v Irgacure 2959. After fabrication, the parts were sterilized in 70% ethanol for 1 hour, followed by storage in phosphate buffered saline (PBS).

2.2 Seeding of C2C12 myoblast rings

C2C12 murine myoblasts transduced to express Channelrhodopsin-2 (ChR2[H134R]) were cultured in growth medium (GM) consisting of Dulbecco’s Modified Eagle Medium with L-glutamine and sodium pyruvate (DMEM, Corning) supplemented with 10% v/v fetal bovine serum (FBS, Lonza), 1% v/v L-glutamine (Cellgro Mediatech), and 1% v/v penicillin-streptomycin (Cellgro Mediatech). Upon reaching approximately 85% confluency, cells were trypsinized and resuspended at a concentration of $1 \times 10^7 \text{ cells mL}^{-1}$ within a matrix mixture of 30% v/v Matrigel (BD Biosciences), 4 mg mL^{-1} fibrinogen (Sigma-Aldrich), and $0.5 \text{ units mg-fibrinogen}^{-1}$ thrombin (Sigma-Aldrich) in growth medium supplemented with 1 mg mL^{-1} aminocaproic acid (ACA, Sigma-Aldrich) (GM+). The cell-matrix suspension ($120 \text{ }\mu\text{L}$) was pipetted into the injection ring mold and incubated at 37°C for 1 hour before being immersed in GM+.

2.3 Differentiation of skeletal muscle biobots

C2C12 myoblast rings were cultured for 3 days post-seeding in GM+ (refreshed daily). After 3 days, the rings were lifted from their molds and transferred to biobot skeletons where they were immersed in differentiation medium consisting of DMEM supplemented with 10% v/v heat inactivated horse serum (HS, Lonza), 1% v/v L-glutamine, 1% v/v penicillin-streptomycin, 1 mg mL⁻¹ ACA, and 50 ng mL⁻¹ human insulin-like growth factor-1 (IGF-1, Sigma Aldrich) (DM++). Differentiation medium was refreshed daily for 7 days post ring transfer.

2.4 Freezing and thawing of undifferentiated myoblast rings

24 hours post-seeding, undifferentiated C2C12 myoblast rings were removed from their molds and placed into cryogenic freezing tubes containing 1 mL warm GM supplemented with 10% v/v dimethyl sulfoxide (DMSO, Fisher). Freezing tubes were placed in alcohol-free freezing containers (CoolCell, Corning) and stored in the -80°C freezer, where they were slowly frozen at a rate of 1°C min⁻¹. After 24 hours in the freezer, the cryogenic freezing tubes were placed in a warm 37°C water bath for approximately 3 min until completely thawed. The rings were then removed from the tubes, rinsed in PBS, and returned to their original ring molds to incubate for 48 hrs at 37°C. GM+ was refreshed daily. On day 4 post-seeding, rings were transferred to biobot skeletons and differentiated for 7 days in DM++.

2.5 Freezing and thawing of differentiated muscle rings

For this set of experiments, the medium was changed to DM++ on day 3 post-seeding of the cell matrix solution on the ring molds. However, muscle rings were left within the ring molds rather

than being transferred to biobot skeletons. On day 10 post-seeding, the central portion of the ring mold was detached from the rest of the mold, so that the structure could be lifted away with a spatula. The central portion of the mold and the surrounding muscle ring was transferred to a cryogenic freezing tube containing 1 mL warm GM with 10% v/v DMSO and frozen at $-1^{\circ}\text{C min}^{-1}$ to -80°C . After 24 hours in the freezer, the tubes were thawed in a warm 37°C water bath and the mold-ring structures were rinsed in PBS. Rings were removed from the molds, transferred to biobot skeletons, and returned to culture in DM++ at 37°C .

2.6 MTS viability assay

MTS solution (CellTiter 96 AQueous One Solution Cell Proliferation Assay, Promega) was thawed in a 37°C water bath and combined with warm DMEM (without phenol red) in a 1:5 volume ratio to form a working reagent. Muscle rings were rinsed in PBS, placed in individual wells of a 24 well plate, and immersed in MTS working reagent. The reaction was allowed to proceed in the dark for 4 hours at 37°C . A microplate reader (Synergy HT, BioTek) was used to measure absorbance at 490 nm, which was then used to calculate relative viability between control and experimental samples.

2.7 Passive tension measurement

Biobots were detached from glass coverslips and placed in a dish of warm, serum-free DMEM. Side-view images of the biobots were used to calculate passive tension by applying the Euler-Bernoulli beam bending theory (Equation 1), as previously described [15].

$$\text{Equation 1: } F_p = \frac{8EI\delta_{max}}{lL^2}$$

F_p is passive tension force, E is the Young's modulus of the PEGDA skeleton (319.4 kPa), I is the moment of inertia of the beam ($\frac{1}{12}bh^3 = 2.77E^{-14} m^4$), δ_{max} is the maximum deflection of the beam, l is the distance between the muscle and the beam, and L is the length of the beam (6 mm) [15].

2.8 Electrical stimulation and active tension measurement

Two platinum electrodes were aligned parallel to the biobot to stimulate the muscle with 20 V, 50 ms pulses at 1 Hz. Videos of biobot muscle contraction were used to calculate active tension through motion tracking and application of a Kelvin-Voigt viscoelasticity model (Equation 2) [15]. The distance between the two pillars of the biobot was tracked over the course of 150 frames (approximately 25 sec depending on frame rate) to calculate strain and determine the time-varying force, calculated by equation 2. The peak values of active tension force were averaged, and the minimum value of active tension force was subtracted from this average peak value to determine the active tension value for each biobot.

$$\text{Equation 2: } \frac{F\alpha}{A} = E\epsilon(t) + \eta \frac{d\epsilon(t)}{dt} = E \frac{\Delta y}{y_0} + \eta \frac{\Delta \epsilon}{\Delta t}$$

$F\alpha$ is the active tension force, A is the contact area between the muscle ring and the bio-bot skeleton, E is the Young's modulus of the PEGDA skeleton (319.4 kPa), Δy is the change in length of the skeleton during a contraction, y_0 is the original length of the skeleton in the passive state, η is the viscosity of the PEGDA skeleton ($5.1 E^{-3} mPa s$), $\Delta \epsilon$ is the change in strain between successive frames, and Δt is the time between frames [15].

2.9 RT-qPCR analysis of myogenic marker expression

Muscle rings were removed from biobot skeletons, rinsed in PBS, and flash-frozen for 5 min in liquid nitrogen to be stored at $-80^\circ C$. Thawed rings were homogenized by vortexing in RLT buffer

(Qiagen) with 10 $\mu\text{L mL}^{-1}$ B-mercaptoethanol and centrifuged using the QIAshredder (Qiagen) column. RNA was extracted using the RNeasy Plus RNA isolation kit (Qiagen) according to the manufacturer's instructions. cDNA synthesis was done using qScript cDNA SuperMix (Quanta Biosciences) from 100 ng of RNA and reactions were performed as directed by the supplier. For RT-qPCR, SsoFast EvaGreen Supermix (Bio-Rad) was added to cDNA and primers targeting the genes of interest and GAPDH (Table 1, Appendix A). The cycling parameters were 30 s at 95 °C, and 40 cycles of 5 s at 95 °C and 20 s at 55 °C, followed by melt-curve analysis of the product using a CFX Connect Real-Time System (Bio-Rad). Cycle threshold (Ct) values were used to calculate changes in expression level, relative to GAPDH and control samples by the $2^{-\Delta\Delta\text{Ct}}$ method [20]. Reaction efficiencies over the appropriate dynamic range were calculated to ensure linearity of the standard curve.

2.10 Immunohistochemical staining and light sheet imaging of muscle rings

Muscle rings to be imaged were rinsed with PBS. To preserve the internal structure, the tissue was fixed on the skeleton structures using 4% v/v of paraformaldehyde for 20 minutes. Samples were later permeabilized using Triton-X, which was diluted to 0.25% v/v and used to permeabilize the tissue membrane for 20 minutes. After washing with PBS, samples were blocked and stored in 1% w/v bovine serum albumin (Sigma Aldrich) diluted in PBST at 4 °C. Cell membrane was immunolabeled with mouse anti-myosin heavy chain (MF-20) and rabbit anti- α -actinin, were used to stain for myosin and the sarcomere respectively. AlexaFluor-647 anti-mouse (ThermoFisher) and AlexaFluor-633 anti-rabbit (ThermoFisher) was used to stain MF-20 and α -actinin primary antibodies respectively and incubated for 2 hrs at room temperature. To be able to image 3D tissue,

stained samples were embedded in 1% agarose inside a 1ml syringe. For imaging, the embedded sample was suspended in a chamber to be imaged by a Zeiss Z1 Lightsheet microscope.

2.11 Quantifying myotube dispersion

The Directionality plugin for ImageJ was used to determine the alignment of myotubes through Fourier component analysis, as previously demonstrated [21]. A histogram was formed by determining the number of myotubes in each direction. A Gaussian fit was calculated from the highest peak, which represents the preferred orientation. The standard deviation of the Gaussian fit is referred to as the dispersion. The α -actinin fluorescent images were used with the Directionality plugin to determine alignment.

2.12 SEM imaging of muscle rings

Muscle rings were rinsed in PBS and fixed in 4% paraformaldehyde (PFA) for 20 minutes. Samples were then rinsed in PBS for 5 minutes, followed by a series of 10 minute immersions in 37%, 67%, and 95% (x3) ethanol to dehydrate the tissue. Afterwards, samples were washed with hexamethyldisilazane and left to dry overnight at room temperature. Samples were then coated with gold palladium prior to adhering to a chuck covered with carbon tape. Mounted samples were imaged in a FEI Quanta FEG 450 ESEM.

2.13 Statistical Analysis

In all bar graphs, data is represented as the mean \pm standard deviation. The students T test was used to determine significance, with $p < .05^*$, $p < .01^{**}$, $p < .001^{***}$.

CHAPTER 3: RESULTS

3.1 Freezing of tissue engineered skeletal muscle

To study the effects of freezing on skeletal muscle, we engineered a versatile ring shaped skeletal muscle bioactuator, originally developed by Raman et al. [15], [16]. Skeletal muscle rings were formed from a cell-gel mixture of C2C12 myoblasts, fibrin, and Matrigel (Fig 1a) which was added to a 3D printed PEGDMA mold (Fig 1b) in order to achieve a ring-like shape. The cell-gel solution compacted within the mold over time to form a dense 3D ring structure. After 3 days within the mold, the tissue ring was removed from the mold and transferred to a 3D printed PEGDA skeleton structure (Fig 1c). The growth medium was changed to a differentiation medium, driving muscle ring differentiation over the course of the next 7 days (Fig 1d). After differentiation of the myoblasts to myotubes, the biobot was electrically stimulated to observe the contraction of the tissue engineered muscle ring. The 3D printed skeleton was designed such that contraction of the muscle ring causes deflection of the beam and the inward bending of the two pillars (Fig 1c). The bending of the skeleton can be measured in order to quantify the force production of the muscle ring, enabling the analysis of the functional performance of the tissue engineered skeletal muscle.

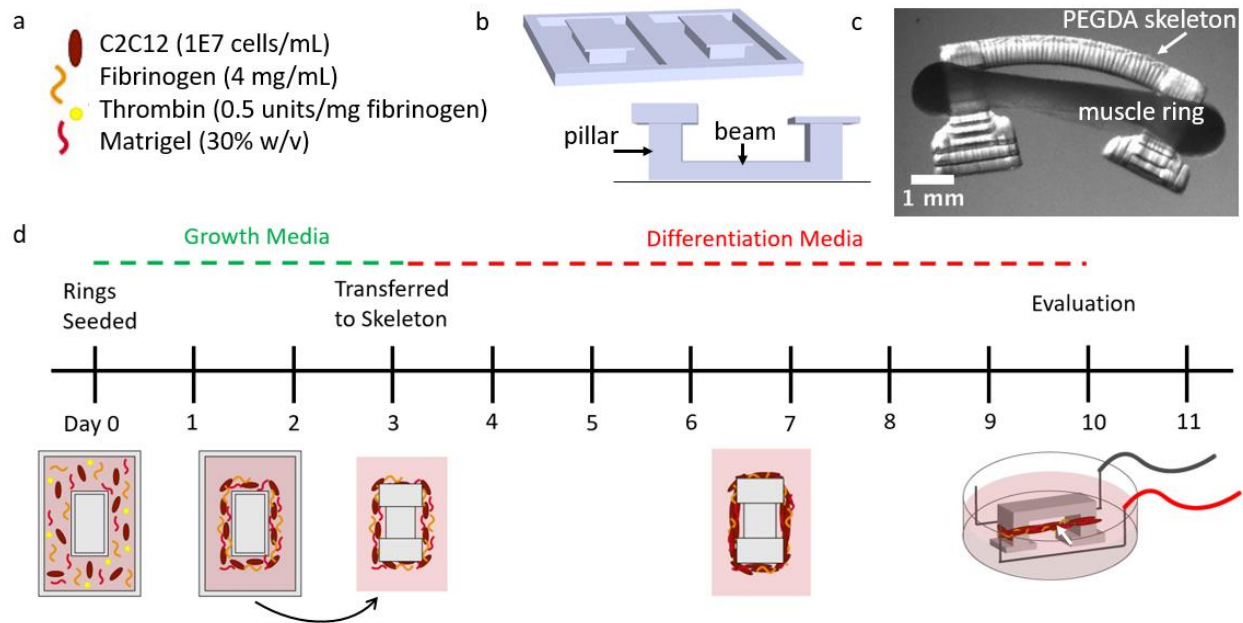


Figure 1. Skeletal muscle bioactuator fabrication. (a) Composition of cell-matrix solution used to form the muscle ring. (b) CAD image of 2 ring molds (top) and the skeleton structure (bottom) which are 3D printed using stereolithography. The skeleton is printed with its beam tethered to the bottom of a glass slide so that the muscle ring remains in tension throughout the differentiation process. (c) Side-view image of the mature bioactuator once it has been released from the glass slide. (d) On day 0, C2C12 myoblasts and matrix gel components are pipetted into a 3D printed PEGDA ring mold. The ring is allowed to solidify and compact in growth media for the next 3 days. On day 3, the compacted ring is removed from the mold and transferred to a 3D printed, asymmetric skeleton structure and the media is changed to differentiation media. On day 10, the skeletal muscle can be placed between two platinum electrodes and electrically stimulated to analyze force production of the mature muscle ring. In its upright position, the asymmetric design of the skeleton allows for unidirectional locomotion of the entire structure.

The engineered muscle ring was frozen at two different time points, before and after differentiation, to determine which method would be optimal for preservation of the skeletal muscle's health and function. To cryopreserve the tissue while undifferentiated, the muscle ring was frozen after 24 hrs post-cell seeding (Fig 2a). The muscle ring was removed from the ring mold and submerged in freezing medium within a cryogenic freezing tube. The ring was found to be mechanically robust enough to withstand removal from the mold without rupture. Similarly, the tissue maintained its ring-like shape throughout the freezing process and could be easily

returned to the ring mold post-thaw, where it was allowed to remain in culture for an additional 2 days before being transferred to the skeleton structure (Fig 2a). The total amount of time in growth medium within the ring mold, and in differentiation medium while attached to the skeleton structure, was identical to that of an unfrozen muscle ring.

The second cryopreservation method involved freezing of the muscle ring after differentiation, 9 days post-cell seeding (Fig 2b). This time point of freezing occurs 2 days after the skeletal muscle rings first exhibit macroscale contraction, indicating the presence of differentiated myotubes [15]. The timeline for muscle differentiation prior to freezing was identical to that of the unfrozen ring. However, rather than transferring the ring to the skeleton structure on day 3, the ring was left to differentiate within the mold. This was done to avoid having to freeze the 3D printed skeleton structure. When the differentiated ring was frozen while attached to the skeleton, the entire structure collapsed inward such that the pillars of the skeleton touched and no contraction of the ring could be visualized (Fig 3a). The process of freezing likely contributed to microstructural changes within the PEGDA that allowed the muscle ring to easily compact the weakened structure once it was thawed. To avoid this issue, we attempted to freeze the differentiated ring by itself, but found that it could not retain its shape throughout the freezing process. The passive tension of the differentiated myotubes caused the ring to compact inward such that the ring was too small to be transferred to the skeleton. To avoid these complications, we removed the elevated central portion of the ring mold along with the muscle ring in order to preserve the shape of the muscle ring throughout the freezing process (Fig 3b,c). After thawing, the muscle ring was simply removed from the mold and transferred to the 3D printed skeleton, where it was cultured for another 24 hrs.

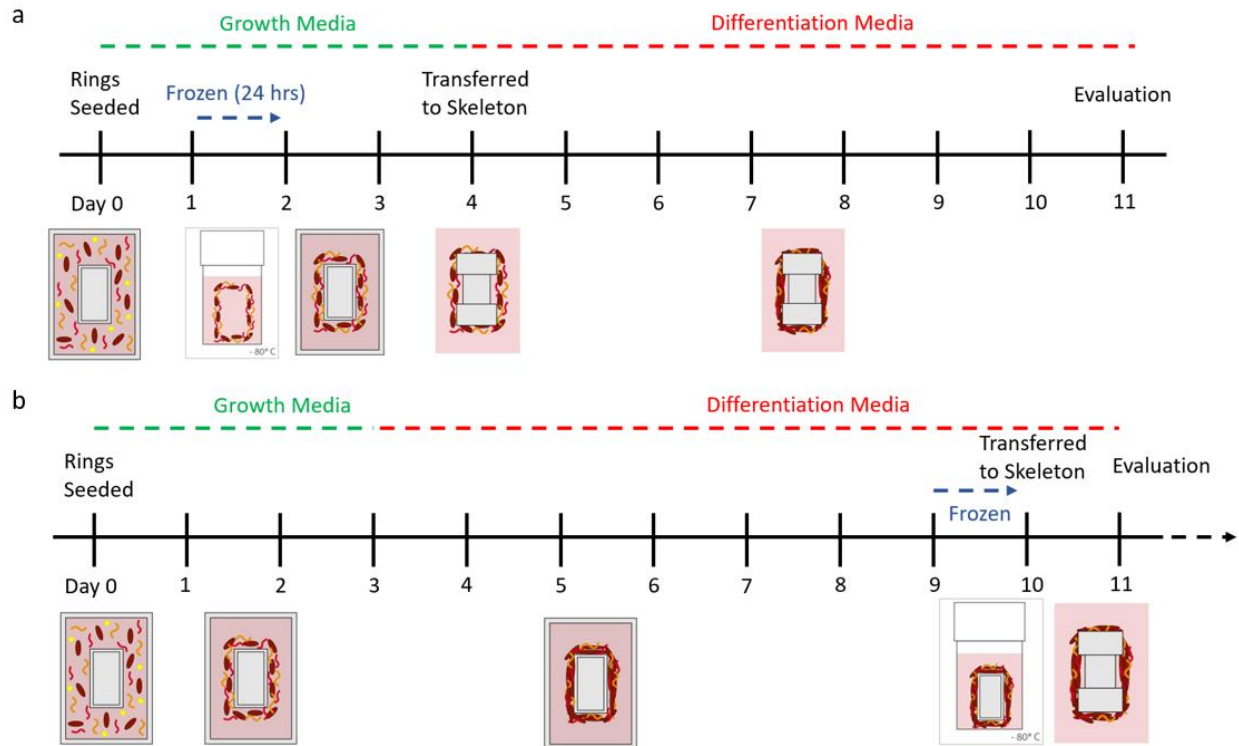


Figure 2. (a) Timeline for freezing of bioactuators before differentiation. 24s hrs post-seeding, the ring is removed from culture and placed in a cryogenic freezing vial with 1 mL of medium. The ring is slowly frozen at -1 deg C/min and left at -80 deg C for 24 hrs. The ring is rapidly thawed for 3 min in a water bath, transferred back to the ring mold, and maintained in culture for 24 hrs. On day 4, the ring is transferred to the skeleton and differentiation begins. Evaluation of the ring occurs on day 11 (rather than day 10) to account for the “null time” while frozen. (b) Timeline for freezing of bioactuators after differentiation. Similar to the standard protocol for bioactuator fabrication, differentiation begins on day 3. However, the muscle ring is differentiated within the ring mold. The entire central region of the ring mold is frozen with the muscle in order to prevent the muscle from losing its shape. After being thawed, the muscle ring is transferred directly from the mold to the skeleton and left in culture to recover at least 24 hrs prior to evaluation.

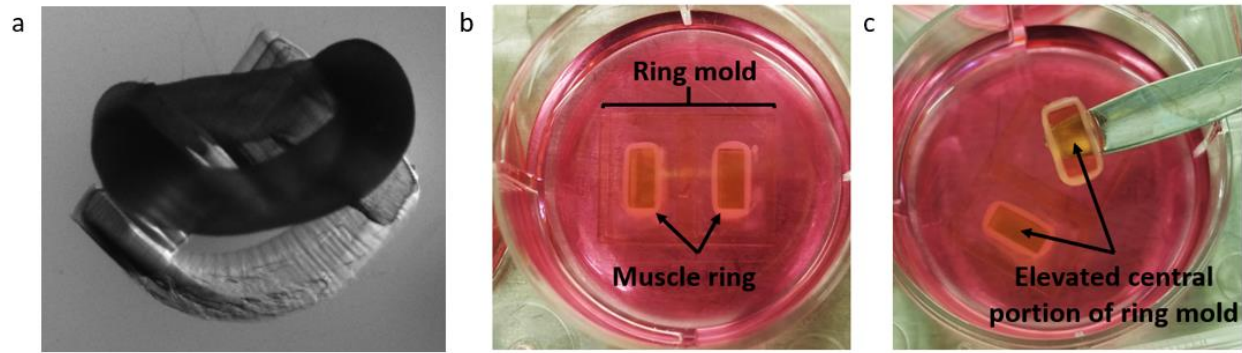


Figure 3. (a) Image of differentiated skeletal muscle which was frozen after transfer to the PEGDA skeleton. The effects of freezing on the PEGDA skeleton caused deflection of the beam such that the pillars came into contact and no active tension could be measured. (b) Image of muscle rings differentiated within the ring mold (c) Image demonstrating how the central portion of the ring mold is detached from the rest of the mold to be frozen with the muscle ring.

3.2 Effect of freezing on cell viability

To effectively freeze and revive biological tissues without incurring a loss of function, it is imperative to prevent significant cell death. In the case of skeletal muscle constructs, a reduction in cell number would lead to a decrease in net force production. Furthermore, the presence of dead cells may impair the process of myoblast differentiation, thus decreasing the maturity and function of single myotubes. In order to examine the effects of freezing on skeletal muscle 3D constructs, we began by first freezing muscle rings in the undifferentiated state (1 day post-cell seeding). MTS viability assays were performed to optimize the freezing medium composition and quantify the effect of the freezing process on cell viability. Undifferentiated muscle rings were frozen in the same growth medium (GM) in which they were cultured. Dimethyl sulfoxide, or DMSO, serves as a cryoprotectant [22] and was supplemented to the freezing medium at concentrations of 5%, 10%, and 15% v/v. Muscle rings were slowly frozen at $-1\text{ }^{\circ}\text{C}/\text{min}$ to -80°C and were thawed rapidly after being frozen for 24 hrs. MTS assays showed that undifferentiated muscle rings frozen in growth medium with 5% DMSO had a viability of $87\% \pm 6.5\%$, rings frozen with 10% DMSO

had a viability of $93\% \pm 8.4\%$, and rings frozen in 15% DMSO had a viability of $84\% \pm 8.0\%$ (Fig 4a). Only the rings frozen in 10% DMSO did not exhibit significantly lowered viability as compared to the unfrozen control. For this reason, all undifferentiated rings in future studies were frozen in growth medium supplemented with 10% DMSO. To examine the effect of total time frozen on cell viability, undifferentiated rings were frozen for periods of 1 day, 1 week, 1 month, and 2 months. MTS viability assays showed that for all time periods, the viability of frozen rings was never significantly lowered, as compared to the unfrozen control (Fig 4b). These results show that growth medium supplemented with 10% DMSO serves as an adequate freezing medium for undifferentiated muscle rings, which can be frozen for long periods of time without a reduction in cell viability.

While undifferentiated muscle rings could be frozen without a significant effect on cell viability, this was not the case for differentiated muscle. When differentiated muscle rings were frozen in differentiation medium (DM) with 10% DMSO, viability was significantly reduced to $73\% \pm 3.9\%$ (Fig 4c). To examine whether this effect may have been due to the use of differentiation medium rather than growth medium for the freezing process, another viability study was conducted to compare differentiated muscle frozen in growth vs differentiation medium (Fig 4d). Differentiated muscle rings frozen in differentiation medium had a viability of $77\% \pm 7.7\%$ while muscle rings frozen in growth medium had a viability of $81\% \pm 6.9\%$. The viability of differentiated muscle rings was significantly reduced when frozen in either medium, and no significant difference between the viability of rings frozen in the two mediums was observed.

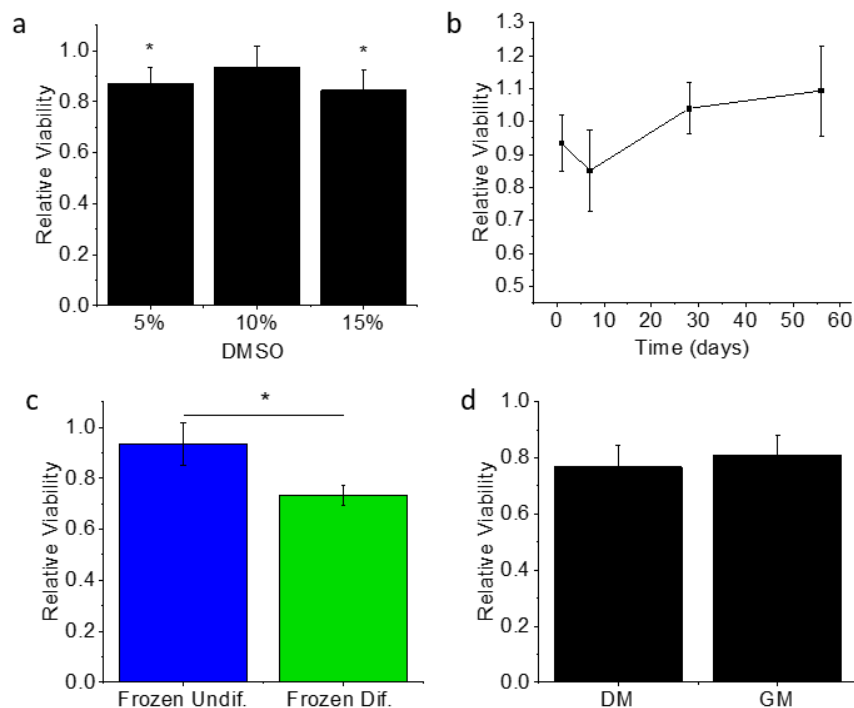


Figure 4. (a) MTS viability of undifferentiated muscle rings after being frozen for 24 hrs in growth medium with varying concentrations of DMSO (n=3). Viability is normalized to that of the unfrozen control. (b) MTS viability of undifferentiated muscle rings after being frozen for varying time periods in growth media with 10% DMSO (n=3). (c) MTS viability of muscle rings frozen after differentiation as compared to muscle rings frozen prior to differentiation (mean \pm SD, n=3). (d) MTS viability of differentiated muscle rings frozen in differentiation media and growth media (n=3). (*p<0.05, **p<0.01)

3.3 Force production of frozen muscle rings

To understand how freezing 3D rings of undifferentiated myoblasts impacts their eventual development into mature myotubes, we began by measuring their force production post-differentiation. Differentiated skeletal muscle rings which had previously been frozen for 24 hrs in the undifferentiated state surprisingly produced significantly higher active contractile force ($174 \pm 82 \mu\text{N}$) than the unfrozen control ($45 \pm 17 \mu\text{N}$) (Fig 5a) (Video 1-2, Appendix B). Passive tension, however, was not affected by the freezing process (Fig 5b). Active and passive tension of a single frozen undifferentiated muscle ring is plotted with time to visualize the change in active force production as the muscle contracts under 1 Hz stimulation (Fig 5c). Muscle rings which had

been frozen also contracted spontaneously, while unfrozen rings did not undergo any spontaneous contraction (Fig 5d) (Video 3, Appendix B).

Skeletal muscle rings which were frozen after differentiation were found to produce significantly lower active tension as compared to the unfrozen and frozen differentiated muscle (Video 4, Appendix B). When frozen rings were allowed to recover for 24 hrs in culture post-thawing, only one out of four frozen muscle rings demonstrated macroscale contraction in response to stimulation ($5.3 \mu\text{N}$) (Fig 5e). When these same four muscle rings were allowed to recover in culture for another 24 hrs (for a total of 48 hrs post-thaw), all muscle rings increased in active tension, by an average of $10 \mu\text{N}$ (Fig 5e). However, even after 2 days of recovery, average active tension of the muscle ($11.7 \pm 8.5 \mu\text{N}$) was still significantly lower than the unfrozen control (Fig 5a). Passive tension, however, was not affected by the freezing process (Fig 5b). Freezing medium composition was altered in an attempt to maintain higher functional performance of the muscle. FBS was increased from 10% to 90%, and DMSO was increased to 20%, but no improvement in force production was achieved (Fig 5f).

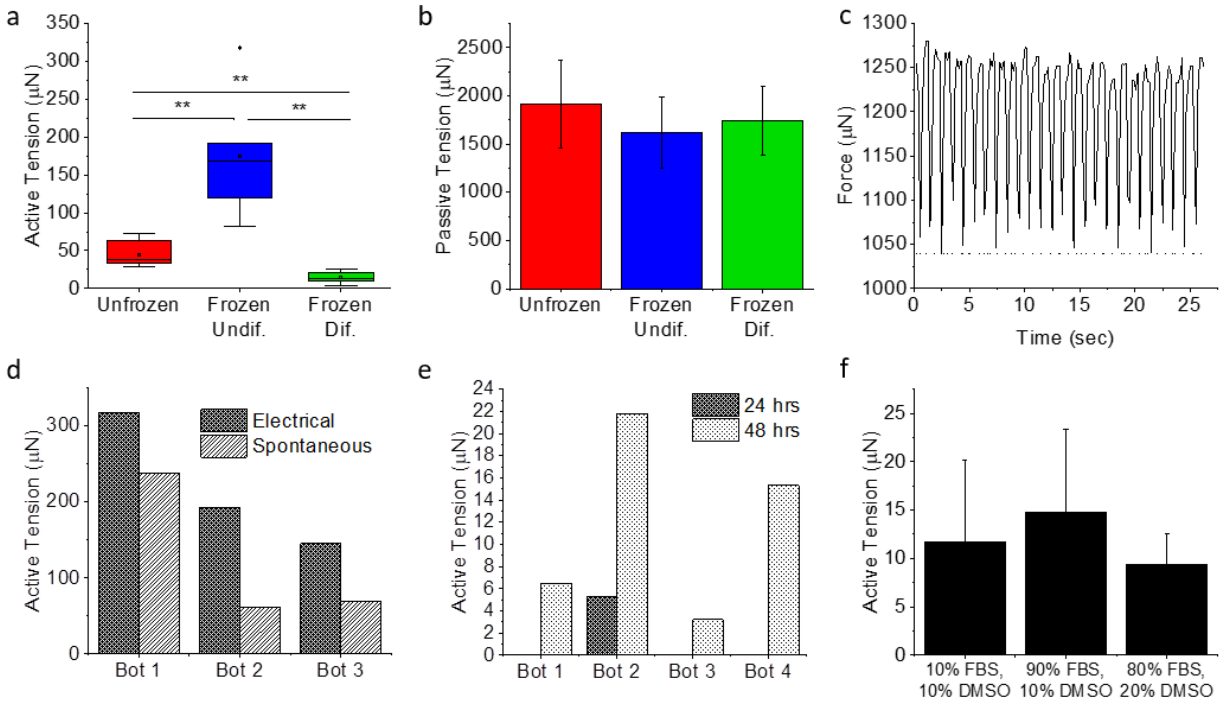


Figure 5. (a) Active tension produced by differentiated skeletal muscle rings stimulated electrically at 1 Hz ($n=7,6,5$). (b) Passive tension of differentiated skeletal muscle rings ($n=7,6,5$). (c) Active tension (solid line) and passive tension (dotted line) plotted with time for a single frozen undifferentiated biobot stimulated at 1 Hz. (d) Electrical and spontaneous active tension measurements of three frozen undifferentiated muscle rings. (e) Active tension of 4 frozen differentiated biobots recovered measured 24 and 48 hrs post-thaw. (f) Freezing media for differentiated muscle was modified to increase FBS and DMSO concentration ($n=3$). (* $p<0.05$, ** $p<0.01$)

3.4 Effect of freezing on myogenic marker expression

To further understand the effects that freezing in the undifferentiated state has on muscle development, and to shed light on the molecular mechanisms which may be responsible for the observed increase in force production, we used RT-qPCR to analyze the changes in gene expression associated with myoblast freezing. The following myogenic markers were measured: desmin, myostatin, myogenic factor 5, myogenic factor 6, myosin heavy chain 1, MyoD, myogenin, and troponin 1. Differentiated muscle rings which had been frozen for 24 hrs in the undifferentiated state showed significantly increased expression of myogenic factor 6 (1.9 ± 0.4

fold) and myosin heavy chain 1 (1.7 ± 0.3 fold), as compared to the unfrozen control (Fig 6a). Myogenic factor 6 (MYF6) is highly expressed in terminally differentiated myotubes or myofibers, and upregulation may indicate that the frozen undifferentiated muscle has achieved a more advanced state of differentiation [23]. Myosin heavy chain 1 (MYH1) is also a late-stage myogenic marker, and is essential for force-generating muscle contraction [24].

RT-qPCR was also used to evaluate the changes in myogenic marker expression associated with the freezing of differentiated muscle. Muscle rings were frozen for 24 hrs in GM with 10% DMSO and were recovered in culture for 48 hrs post-thawing. Increased expression of desmin (1.7 ± 0.3 fold), myogenic factor 5 (1.5 ± 0.1 fold), MyoD (2.5 ± 0.7 fold), and myogenin (2.0 ± 0.1 fold) was observed, while MYF6 showed decreased expression (0.5 ± 0.1 fold), as compared to the unfrozen control (Fig 6b). Increased expression of early stage myogenic markers (MYOD, MYF5, and DES) and mid-stage myogenic marker MYOG, together with decreased expression of terminal differentiation marker MYF6, could indicate a relative increase in the presence of myoblasts as compared to mature myotubes [24]. Compared to the frozen undifferentiated muscle, frozen differentiated muscle exhibits significantly higher expression of MYF5, MYOD, and MYOG and lower expression of MYF6 (Fig 6c).

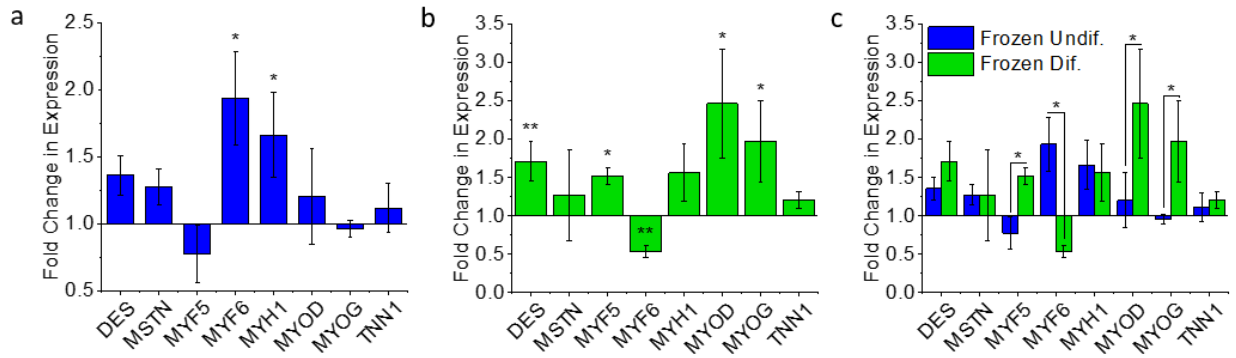


Figure 6. (a) RT-qPCR fold change in mRNA expression of various myogenic markers in differentiated muscle which had previously been frozen while undifferentiated. Expression is normalized to the unfrozen control (mean \pm SD, n=3). (b) RT-qPCR fold change in mRNA expression in muscle frozen differentiated (mean \pm SD, n=3). (c) Comparison of gene expression in frozen undifferentiated and frozen differentiated muscle, each normalized to unfrozen controls (mean \pm SD, n=3). (*p<0.05, **p<0.01)

3.5 Effect of freezing on myotube structure

To visualize any changes to myotube structure caused by the freezing process, skeletal muscle samples were labeled for α -actinin, myosin, and cell nucleus (DAPI) (Fig 7a-c). Light sheet microscopy was used to analyze myotube alignment, thickness, and striation, which all play a critical role in the force generation of 3D skeletal muscle tissue [1]. Mature muscle rings which had been frozen while undifferentiated showed a dispersion angle of $10.1 \pm 2.8^\circ$ as compared to the unfrozen control $9.3 \pm 2.1^\circ$, indicating no effect of freezing in the undifferentiated state to the development of aligned myotubes (Fig 8a). The average myotube width of the frozen undifferentiated muscle rings ($10.1 \pm 0.4 \mu\text{m}$) was similar to that of the unfrozen tissue ($8.6 \pm 1.2 \mu\text{m}$) (Fig 8b). Both the unfrozen and frozen undifferentiated tissues contained visibly striated myotubes as indicated by the α -actinin stain, with sarcomere intervals of 1.2 ± 0.02 and $1.2 \pm 0.03 \mu\text{m}$, respectively (Fig 8c,d).

Muscle rings which had been frozen after differentiation, however, had a significantly higher dispersion angle of 15.7 ± 6.2 . Compared to both the frozen undifferentiated and unfrozen

muscle rings, the increase in dispersion was significantly higher, indicating a disruption to myotube alignment caused by the process of freezing differentiated muscle (Fig 8a). The average myotube width within the frozen tissue was $8.6 \pm 0.8 \mu\text{m}$, similar to that of the unfrozen tissue, but significantly lower than that of the frozen undifferentiated muscle (Fig 8b). Frozen differentiated myotubes also showed striation, with an average sarcomere interval of $1.1 \pm 0.12 \mu\text{m}$, similar to that of the unfrozen and frozen undifferentiated tissues, indicating no decrease in the force generation capability of individual myotubes (Fig 8d) [25], [26].

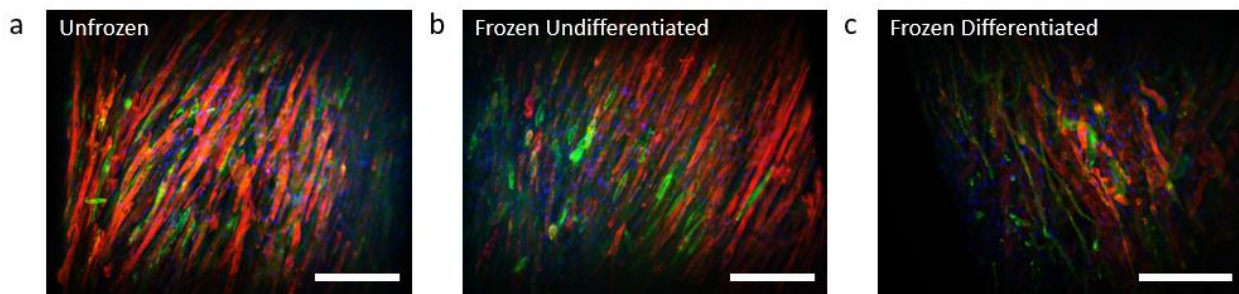


Figure 7. (a-c) Light sheet images of differentiated skeletal muscle rings stained with α -actinin (red), myosin (green), and DAPI (blue). Scale bar = $100 \mu\text{m}$.

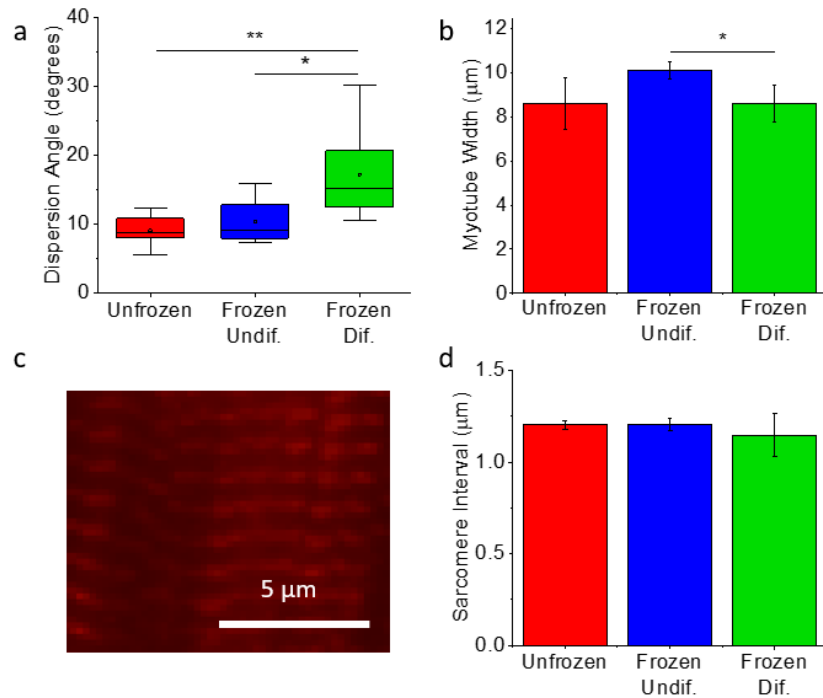


Figure 8. (a) Dispersion angle of myotube directionality shows loss of myotube alignment in frozen differentiated muscle (n=12) as compared to unfrozen muscle (n=10) and frozen undifferentiated muscle (n=11). (b) Average myotube width obtained by measuring the widest diameter of 10 random myotubes within each muscle ring image (mean \pm SD, n=3). (c) Magnified image of a bundle of myotubes within a frozen undifferentiated muscle ring, showing clearly distinguished striation indicated by α -actinin bands. (d) Sarcomere interval measured by calculating the distance between α -actinin bands in light sheet images. (*p<0.05, **p<0.01)

3.6 Effect of freezing on ECM microstructure

To further understand the mechanism by which the process of freezing undifferentiated muscle rings promotes the development of mature muscle with increased force production, we investigated the structure of the extracellular matrix. We used SEM to image the surface structure of both unfrozen muscle rings and muscle rings which were frozen in the undifferentiated state. Unfrozen, undifferentiated samples appeared to have a thick, smooth matrix coating along the surface of the ring (Fig 9a), while undifferentiated muscle rings which had been frozen seemed to show an apparent thinning of the matrix (Fig 9b). By the time rings which had been frozen in the

undifferentiated state were allowed to differentiate, however, their surfaces seemed to be smoother. There was no distinguishable difference between the matrices of the frozen vs unfrozen differentiated muscle rings after differentiation (Fig 9c,d).

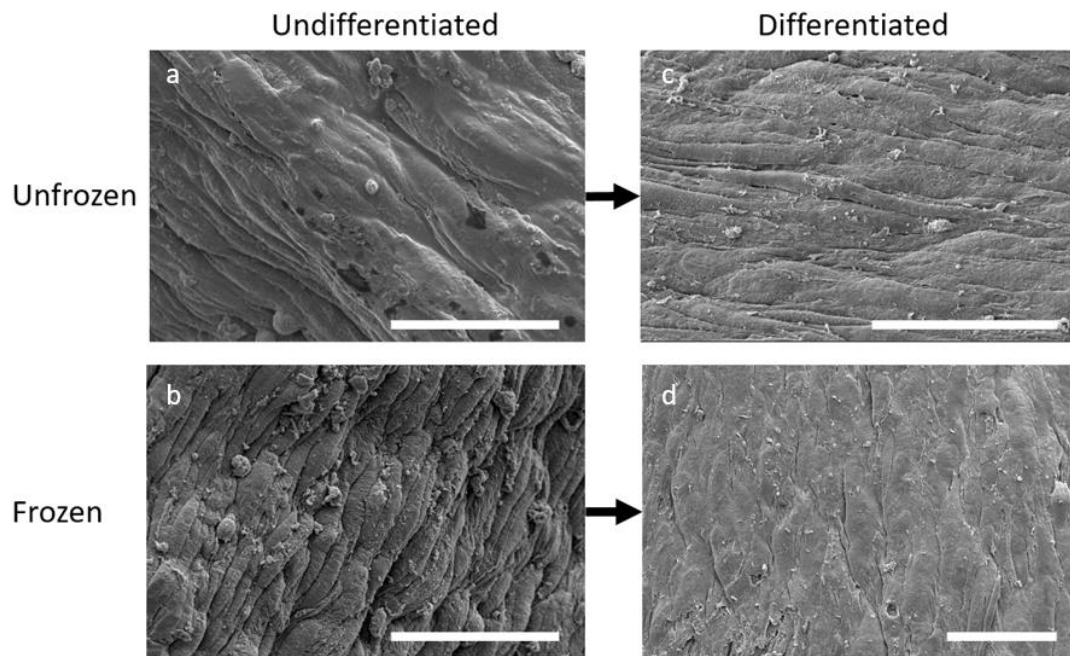


Figure 9. SEM images of muscle ring surface. (a) Unfrozen, undifferentiated muscle ring, showing appearance of thick ECM coating. (b) Frozen, undifferentiated muscle ring, showing apparent thinning of ECM coating as compared to the unfrozen, undifferentiated muscle. (c) Unfrozen, differentiated muscle ring. (d) Differentiated muscle ring which had been previously frozen while undifferentiated, showing ECM coating similar in appearance to that of the unfrozen, differentiated muscle.

CHAPTER 4: DISCUSSION

Cryopreservation serves as an effective method for the long-term storage of living cells for many applications. However, the process of freezing is known to have many detrimental effects on living cells. Osmotic intolerance, toxicity of cryoprotectants, chilling or cold-shock, and intracellular ice formation can all contribute to cell death or loss of function as cells undergo the freeze-thaw process [27]. These negative effects are especially apparent in the freezing of bulk tissues, which possess differing heat and mass transfer effects that prevent even temperature and cryoprotectant distribution. Our results were consistent in showing the process of freezing to have negligible effects on 3D constructs of undifferentiated myoblasts, but a much more detrimental effect when freezing occurred after the 3D constructs had been differentiated into a dense skeletal muscle tissue.

The process of cryopreserving differentiated skeletal muscle not only lowered cell viability, but also caused a loss of myotube alignment, which likely both contributed to the resulting loss of function as demonstrated by the significantly decreased force production [21]. Skeletal muscle which had been frozen while differentiated showed increased expression of MYOD, which is known to activate in response to cell damage, and can even induce cell apoptosis. Desmin is a protein which helps maintain sarcomere alignment and regulate muscle contraction, and its increased expression could indicate a defense mechanism as the frozen myotubes attempt to maintain alignment, which was disrupted by the freezing process. Even after efforts to alter freezing medium composition and allow the muscle rings to recover for up to 48 hrs in medium post-thawing, functional performance of the muscle could not be recovered after freezing. For this

reason, we do not recommend the cryopreservation of tissue engineered skeletal muscle post-differentiation.

After freezing skeletal muscle constructs while undifferentiated, we were surprised to observe an increase in functional performance of the resulting differentiated skeletal muscle. Active tension was increased, as was the expression of myosin heavy chain 1, which is integral in the process of skeletal muscle contraction. Myogenic factor 6 expression was also increased, indicating late stage differentiation as myotubes begin to form myofibers. Myotube alignment was maintained, and myotube width was significantly higher than that of the frozen differentiated muscle. Overall, the process of freezing skeletal muscle constructs prior to differentiation increased muscle performance, and thus, we recommend the protocol indicated in Figure 2a for the optimal freezing of tissue engineered skeletal muscle. Using this protocol, tissue engineered skeletal muscle rings can be efficiently fabricated in large batches and stored for future use, eliminating the time-consuming process of preparing 3D printed molds, expanding C2C12 cell cultures, and seeding the cell-gel solution each time a skeletal muscle tissue is needed for experimentation. This fabrication efficiency could facilitate the integration of bioactuators into laboratory courses to train the next generation of engineers to build systems using biological materials [28]. Similarly, skeletal muscle tissue rings could be fabricated by one lab, then frozen and shipped to various locations for further applications. Once received, the frozen muscle ring would simply need to be thawed and cultured in differentiation medium, making this a simple method for laboratories without tissue engineering expertise to integrate skeletal muscle tissues within their research. The ability to ship pre-made bioactuators would be instrumental for the advancement of skeletal muscle-powered robotics, as many robotics-focused research groups may not have the experience or resources required for tissue engineering. Similarly, the efficient

fabrication and shipment of large batches of muscle tissues may prove useful in pre-clinical drug testing applications, or in future clinical studies in which the tissue engineered skeletal muscle is grafted *in vivo* for the repair of functional muscle [28].

The goal of this study was to optimize a protocol for the cryopreservation of tissue engineered skeletal muscle and characterize the effects of freezing on the muscle. However, the surprising discovery that freezing of undifferentiated muscle tissue leads to enhanced functional performance of the differentiated muscle may prove to be equally impactful. Currently, tissue engineering efforts have not been able to attain the morphology and level of differentiation found in native skeletal muscle, resulting in low force generation and little clinical utility [2]. The mechanisms by which this freezing-induced enhancement of force generation occurs may lead to breakthroughs in the engineering of more highly differentiated and clinically relevant skeletal muscle. However, further studies are necessary to determine the exact mechanisms by which the freezing-induced changes occur.

It is known that tissue engineering scaffolds can be tuned in many ways to optimize the growth and development of seeded cells. Pore size of the scaffold material, for instance, is known to play a critical role in cell attachment and outgrowth, oxygen transfer, and perfusion of nutrients and waste [29]. In the case of myoblast differentiation, it has been shown that matrices with elongated pores induce the formation of more aligned myotubes capable of higher net force production, while also increasing the efficiency of myotube formation [30]. We believe that the ice crystal formation associated with the freezing process may have caused changes to the microstructure of the tissue's ECM. The process of freezing ECM has been previously demonstrated to increase collagen network pore size, in addition to increasing fibril diameter [31]. An increase in porosity of the ECM of frozen undifferentiated muscle may have enabled the more

efficient cell migration and fusion, leading to the formation of a more mature myotubes capable of higher force production. The SEM images in Figure 5 indicate a change to the ECM structure caused by the freezing of undifferentiated muscle tissue. The observation of a thinned ECM in the frozen undifferentiated tissue, which appears to recover in thickness by the time the tissue has differentiated, may suggest the frozen undifferentiated muscle was able to secrete its own matrix. This increase in ECM secretion may have been stimulated by the freezing-induced increase in pore size, which has previously been shown to stimulate the increased ECM secretion of chondrocytes [32]. Furthermore, ECM composition is known to affect skeletal muscle force generation, and the naturally secreted matrix was likely optimal for the development of stronger muscle tissues [17]. However, further studies are needed to confirm this hypothesis and analyze the effects of pore size and ECM fibril thickness on muscle differentiation. Similarly, imaging of the microstructure throughout the 3D tissue and analysis of ECM composition differences in frozen and unfrozen muscle will be necessary to examine the effects of freezing on the ECM.

CHAPTER 5: CONCLUSIONS AND FUTURE DIRECTIONS

In this study, we optimized a protocol for the cryopreservation of tissue engineered skeletal muscle constructs prior to differentiation. This protocol not only maintains cell viability, myotube structure, and alignment, and but also leads to increased force generation as well as the increased expression of late-stage myogenic markers. Further studies are needed to determine the mechanisms by which the freezing of undifferentiated muscle tissue leads to the differentiation of stronger skeletal muscle. Specifically, studies which examine the effects of freezing on ECM and role of these ECM changes in myogenesis may advance the engineering of stronger, more efficient skeletal muscle. The ability to freeze and ship tissue engineered skeletal muscle, as well as the resulting increase in force production, will help drive the advancement of clinical and robotic applications of engineered skeletal muscle tissues.

REFERENCES

- [1] S. Ostrovidov *et al.*, “Skeletal Muscle Tissue Engineering: Methods to Form Skeletal Myotubes and Their Applications,” *Tissue Eng. Part B Rev.*, vol. 20, no. 5, pp. 403–436, 2014.
- [2] W. Bian and N. Bursac, “Tissue engineering of functional skeletal muscle: Challenges and recent advances,” *IEEE Engineering in Medicine and Biology Magazine*, vol. 27, no. 5, pp. 109–113, 2008.
- [3] S. G. M. Uzel, A. Pavesi, and R. D. Kamm, “Microfabrication and microfluidics for muscle tissue models,” *Progress in Biophysics and Molecular Biology*, vol. 115, no. 2–3, pp. 279–293, 2014.
- [4] A. S. T. Smith, J. Davis, G. Lee, D. L. Mack, and D. H. Kim, “Muscular dystrophy in a dish: engineered human skeletal muscle mimetics for disease modeling and drug discovery,” *Drug Discov. Today*, vol. 21, no. 9, pp. 1387–1398, 2016.
- [5] R. Raman *et al.*, “Damage, Healing, and Remodeling in Optogenetic Skeletal Muscle Bioactuators,” *Adv. Healthc. Mater.*, vol. 6, no. 12, 2017.
- [6] S. G. M. Uzel *et al.*, “Microfluidic device for the formation of optically excitable, three-dimensional, compartmentalized motor units,” *Sci. Adv.*, vol. 2, no. 8, 2016.
- [7] C. Cvetkovic, M. H. Rich, R. Raman, H. Kong, and R. Bashir, “A 3D-printed platform for modular neuromuscular motor units,” *Microsystems Nanoeng.*, vol. 3, p. 17015, 2017.
- [8] R. M. Duffy and A. W. Feinberg, “Engineered skeletal muscle tissue for soft robotics: Fabrication strategies, current applications, and future challenges,” *Wiley Interdiscip. Rev. Nanomedicine Nanobiotechnology*, vol. 6, no. 2, pp. 178–195, 2014.
- [9] L. Ricotti *et al.*, “Biohybrid actuators for robotics: A review of devices actuated by living cells,” *Sci. Robot.*, vol. 2, no. 12, p. eaaq0495, 2017.
- [10] R. Raman and R. Bashir, “Biomimicry, Biofabrication, and Biohybrid Systems: The Emergence and Evolution of Biological Design,” *Adv. Healthc. Mater.*, vol. 6, no. 20, 2017.
- [11] C. Cvetkovic *et al.*, “Three-dimensionally printed biological machines powered by skeletal muscle,” *Proc. Natl. Acad. Sci.*, vol. 111, no. 28, pp. 10125–10130, 2014.
- [12] P. Mazur, “Freezing of living cells: mechanisms and implications.,” *Am. J. Physiol.*, vol. 247, no. 3 Pt 1, pp. C125–C142, 1984.
- [13] A. G. E. Day, K. S. Bhangra, C. Murray-Dunning, L. Stevanato, and J. B. Phillips, “The Effect of Hypothermic and Cryogenic Preservation on Engineered Neural Tissue,” *Tissue Eng. Part C Methods*, vol. 23, no. 10, pp. 575–582, 2017.
- [14] B. P. Best, “Cryoprotectant Toxicity: Facts, Issues, and Questions,” *Rejuvenation Res.*, vol. 18, no. 5, pp. 422–436, 2015.
- [15] R. Raman, C. Cvetkovic, and R. Bashir, “A modular approach to the design, fabrication, and characterization of muscle-powered biological machines,” *Nat. Protoc.*, vol. 12, no. 3, pp. 519–533, 2017.
- [16] R. Raman *et al.*, “Optogenetic skeletal muscle-powered adaptive biological machines,” *Proc. Natl. Acad. Sci.*, vol. 113, no. 13, pp. 3497–3502, 2016.
- [17] S. Hinds, W. Bian, R. G. Dennis, and N. Bursac, “The role of extracellular matrix composition in structure and function of bioengineered skeletal muscle,” *Biomaterials*, vol. 32, no. 14, pp. 3575–3583, 2011.
- [18] R. G. Dennis, P. E. Kosnik, M. E. Gilbert, and J. a Faulkner, “Excitability and contractility

- of skeletal muscle engineered from primary cultures and cell lines.," *Am. J. Physiol. Cell Physiol.*, vol. 280, no. 2, pp. C288–C295, 2001.
- [19] M. S. Sakar *et al.*, "Formation and optogenetic control of engineered 3D skeletal muscle bioactuators," *Lab Chip*, vol. 12, no. 23, p. 4976, 2012.
- [20] K. J. Livak and T. D. Schmittgen, "Analysis of relative gene expression data using real-time quantitative PCR and the 2(-Delta Delta C(T)) Method.," *Methods*, vol. 25, no. 4, pp. 402–8, 2001.
- [21] G. J. Pagan-Diaz *et al.*, "Simulation and Fabrication of Stronger, Larger, and Faster Walking Biohybrid Machines," *Adv. Funct. Mater.*, vol. 28, no. 23, p. 1801145, Jun. 2018.
- [22] L. E. McGann and M. L. Walterson, "Cryoprotection by dimethyl sulfoxide and dimethyl sulfone," *Cryobiology*, vol. 24, no. 1, pp. 11–16, 1987.
- [23] P. S. Zammit, "Function of the myogenic regulatory factors Myf5, MyoD, Myogenin and MRF4 in skeletal muscle, satellite cells and regenerative myogenesis," *Seminars in Cell and Developmental Biology*, vol. 72, pp. 19–32, 2017.
- [24] J. A. Dominov, J. J. Dunn, and J. B. Miller, "Bcl-2 expression identifies an early stage of myogenesis and promotes clonal expansion of muscle cells," *J. Cell Biol.*, vol. 142, no. 2, pp. 537–544, 1998.
- [25] H. E. ter Keurs, T. Iwazumi, and G. H. Pollack, "The sarcomere length-tension relation in skeletal muscle," *J. Gen. Physiol.*, vol. 72, no. 4, pp. 565–592, 1978.
- [26] S. B. Lemke and F. Schnorrer, "Mechanical forces during muscle development," *Mechanisms of Development*, vol. 144, pp. 92–101, 2017.
- [27] E. J. Woods, S. Thirumala, S. S. Badhe-Buchanan, D. Clarke, and A. J. Mathew, "Off the shelf cellular therapeutics: Factors to consider during cryopreservation and storage of human cells for clinical use," *Cytotherapy*, vol. 18, no. 6, pp. 697–711, 2016.
- [28] M. Juhas, J. Ye, and N. Bursac, "Design, evaluation, and application of engineered skeletal muscle," *Methods*, vol. 99, pp. 81–90, 2016.
- [29] Q. L. Loh and C. Choong, "Three-Dimensional Scaffolds for Tissue Engineering Applications: Role of Porosity and Pore Size," *Tissue Eng. Part B Rev.*, vol. 19, no. 6, pp. 485–502, 2013.
- [30] W. Bian, M. Juhas, T. W. Pfeiler, and N. Bursac, "Local Tissue Geometry Determines Contractile Force Generation of Engineered Muscle Networks," *Tissue Eng. Part A*, vol. 18, no. 9–10, pp. 957–967, 2012.
- [31] B. Han, J. D. Miller, and J. K. Jung, "Freezing-Induced Fluid-Matrix Interaction in Poroelastic Material," *J. Biomech. Eng.*, vol. 131, no. 2, p. 021002, 2009.
- [32] S. M. Lien, L. Y. Ko, and T. J. Huang, "Effect of pore size on ECM secretion and cell growth in gelatin scaffold for articular cartilage tissue engineering," *Acta Biomater.*, vol. 5, no. 2, pp. 670–679, 2009.

APPENDIX A: RT-QPCR PRIMER SEQUENCES

Table 1. Primer sequences used for RT-qPCR.

Target	Forward Primer (5'-3')	Reverse Primer (5'-3')
GAPDH	CATCACCATCTTCCAGGAGCGA	GTGGTTCACACCCATCACAAACA
DES	CAGTATGAGACCATCGCGGCTA	GCAGGTGTAGGACTGGATCTGG
MSTN	ACAGCCTGAATCCAACCTTAGGCA	CTCATCGCAGTCAAGCCCAAAG
MYF5	ATGTAACAGCCCTGTCTGGTCC	GAGAGAGGGAAGCTGTGTCCTG
MYF6	TTCTTGAGGGTGCGGATTCCT	GGGAGTTTGCGTTCCTCTGAAG
MYH1	TGCAGAGCAAGATTGAGGACGA	CCAGCTTCTTCCAGCCTCTCG
MYOD	TCCAACCTGCTCTGATGGCATGA	CCTCACTGTAGTAGGCGGTGTC
MYOG	CAGTGAATGCAACTCCCACAGC	CTCAGTTGGGCATGGTTTCGTC
TNN1	GGTGGATGAGGAGCGCTATGAT	AGATCCATGGACACCTTGTGCT

APPENDIX B: BIOBOT VIDEOS

Video 1. This supplementary file includes the video “**Unfrozen 1 Hz Electrical Stimulation**” which shows the contraction of an unfrozen biobot under 1 Hz electrical stimulation.

Video 2. This supplementary file includes the video “**Frozen Undifferentiated 1 Hz Electrical Stimulation**” which shows the contraction of a frozen undifferentiated biobot under 1 Hz electrical stimulation.

Video 3. This supplementary file includes the video “**Frozen Undifferentiated Spontaneous**” which shows the spontaneous contraction of a frozen undifferentiated biobot with no electrical stimulation.

Video 4. This supplementary file includes the video “**Frozen Differentiated 1 Hz Electrical Stimulation**” which shows the contraction of a frozen differentiated biobot under 1 Hz electrical stimulation after 2 days recovery post-thaw.